Approximate treatment of density gradients in Rayleigh-Taylor instabilities

Karnig O. Mikaelian
Lawrence Livermore National Laboratory, University of California, Livermore, California 94550
(Received 11 March 1985)

We present an approximate method, based on a moment equation, to derive explicit analytic formulas for the growth rate of Rayleigh-Taylor instabilities in fluids with density gradients. We illustrate with several examples and compare the results with our earlier method of treating a continuous density profile as a large number of fluid layers. The emphasis is on obtaining simple analytic formulas for the largest growth rate.

I. INTRODUCTION

The Rayleigh-Taylor (RT) instability[1,2] occurs at the interface of two fluids subjected to an acceleration directed from the lower to the higher density fluid. The classical case refers to the density profile

$$\rho(y)=\begin{cases}\rho_1, & y<0\\ \rho_2, & y>0\end{cases} \tag{1}$$

with $\rho_1<\rho_2$, and a constant acceleration $\mathbf{g}$ directed from ρ_1 to ρ_2. Perturbations at the interface $y=0$ grow exponentially in time with the classical rate

$$\gamma_{\text{class}}=\left[\frac{gk(\rho_2-\rho_1)}{\rho_2+\rho_1}\right]^{1/2}, \tag{2}$$

where $k=2\pi/\lambda$, λ being the wavelength of perturbation.

Interest in the RT instability has been recently revived because of its important effect in inertial confinement fusion[3,4] (ICF). Imperfections on the surface of a shell can grow large and cause the shell to break up or to mix with the fuel. A number of calculations[4] and experiments[5] have shown that ablation tends to suppress the growth rate. Density gradients occur naturally in these calculations and experiments, and it is well known[6] that density gradients also have the effect of reducing the growth rate of RT instabilities, particularly at short wavelengths. The fact that the shell has a finite thickness also tends to suppress the RT instability, in this case at longer wavelengths.

ICF capsules directly driven by lasers tend to have sharp density gradients while other drivers, e.g., heavy-ion drivers, can induce a more gradual slope in the density profile and benefit from this stabilizing effect. Furthermore, present ICF designs call for rather thin shells, and hence their finite thickness should play a role independently of how they are driven.

Earlier we presented[7] a method for calculating the growth rates in a system which consists of any number N of stratified fluids. While that method is adequate for the study of shells of finite thickness and arbitrary density profiles, it does not yield simple closed-form expressions except in a few simple cases with $N\leq 5$. Continuous density profiles, in particular, are approximated by a large number N of fluid layers, and since the method invokes finding the eigenvalues of an $(N-1)\times(N-1)$ matrix, no analytic form can be written down.

Of course in most (practically all) cases there *is no* such analytic form. However, we found it useful to derive approximate analytic formulas based on a moment equation, and to check them against our earlier method. These formulas are useful as a simple and quick estimate of growth rates as functions of density profile and perturbation wavelength.

This investigation began when we discovered that the result presented in Ref. 6 differed from the result that one obtains using an equation derived by Chandrasekhar (see Ref. 8, Chap. X, Eq. 44): The two results agree in the long-wavelength limit but disagree, by a factor of 2, in the short-wavelength limit. We found that these were special cases of a more general equation that can be appropriately called a moment equation, and that the difference stems from using, as in Ref. 6, an *approximate* rather than an exact eigenfunction.

In the remainder of this paper we present the general moment equation, apply it to several density profiles, and make some concluding remarks.

II. MOMENT EQUATION: DERIVATION AND DISCUSSION

Given a density profile $\rho(y)$, one finds the growth rate(s) γ by solving the second-order differential equation[8] ($D\equiv d/dy$)

$$D(\rho DW)+\frac{gk^2}{\gamma^2}W D\rho-k^2\rho W=0 \tag{3}$$

subject to appropriate boundary conditions. $W(y)$ is an eigenfunction associated with γ and, in general, there are infinitely many growth rates and associated eigenfunctions. In deriving Eq. (3) the assumptions of linearity, incompressibility, and the absence of viscosity, surface tension, and heat transfer are made (see Chap. X in Ref. 8).

Since Eq. (3) can be solved analytically for only a limited number of density profiles, we must use approximation techniques. Multiplying Eq. (3) by W^m and integrating over y, we obtain

$$\frac{\gamma^2}{gk^2}=\frac{\int W^{m+1}D\rho\,dy}{k^2\int\rho W^{m+1}dy+m\int W^{m-1}\rho(DW)^2dy}\ . \tag{4}$$

The integration is over $-\infty\le y\le\infty$ and we have eliminated "surface terms" $\rho W^m DW$ evaluated at $y=\pm\infty$. The exponent m is taken to be a non-negative number, but not necessarily an integer. We refer to Eq. (4) as the moment equation.

Equation (4) reduces to

$$\frac{\gamma^2}{g}=\frac{\int W D\rho\,dy}{\int W\rho\,dy} \tag{5}$$

for $m=0$ and

$$\frac{\gamma^2}{gk^2}=\frac{\int W^2 D\rho\,dy}{k^2\int\rho W^2dy+\int\rho(DW)^2dy} \tag{6}$$

for $m=1$.

Equation (5) shows that there is an upper bound to the growth rate in the general class of continuous density profiles with no free surfaces:

$$\frac{\gamma^2}{g}\le\frac{(D\rho)_{\max}}{\rho_{\min}}\ , \tag{7}$$

where $(D\rho)_{\max}$ is the maximum slope of the profile (finite because ρ is continuous) and $\rho_{\min}$ is the minimum density (nonzero because there are no free surfaces). Equation (7) is significant because it is independent of k and it shows that the growth rate in such density profiles remains finite even in the limit of very short wavelength: compare Eq. (7) with Eq. (2), where $\gamma\to\infty$ as $k=2\pi/\lambda\to\infty$.

Clearly, Eq. (4) will yield the same γ for any m as long as the exact W is used. When an approximate W is used then γ depends on m, which we indicate by $\gamma_{[m]}$.

In the remainder of this paper we choose $W_{\rm class}$ (class denotes classical) as our approximate eigenfunction W in all cases:

$$W_{\rm class}=e^{-k|y-y^*|}\ , \tag{8}$$

where y^* denotes the location of the peak of the eigenfunction [$y^*=0$ for the profile of Eq. (1)]. An important consideration was its simplicity, since we shall integrate over it. Second, it has the proper behavior if $\rho(y)\to$const as $y\to\pm\infty$. As we will see in our applications, the relatively simple expressions that we derive using Eq. (8) agree quite well with the numerical results where a large number N is used to simulate each particular density profile.

It is straightforward to show that $W_{\rm class}$ cannot be an exact eigenfunction for continuous density profiles, and hence the answer will depend on m. We can, however, derive a simple relation between $\gamma_{[0]}$ and $\gamma_{[m]}$ valid for *all* density profiles. Since $W_{\rm class}$ satisfies $W^m(k)=W(mk)$ and $(DW)^2=k^2W^2$, it follows that

$$\gamma^2_{[m]}(k)=\frac{1}{m+1}\gamma^2_{[0]}((m+1)k)\ , \tag{9}$$

so we need to calculate only $\gamma_{[0]}$.

If we were to insist that γ be an exact expression for some density profile and hence be independent of m, we would see from Eq. (9) that this is possible only if $\gamma^2=kF(\rho)$, where F is an arbitrary functional of ρ independent of k. Indeed, the classical γ has exactly this form, which is not surprising since Eq. (8) is the exact eigenfunction for that density profile. The form $\gamma^2=kF(\rho)$, however, violates Eq. (7), which sets an upper bound for the growth rate independent of k. This contradiction is only a reflection of the fact that $W_{\rm class}$ is *not* an exact eigenfunction for continuous density profiles, and we will indeed find that γ depends on m, and the bound Eq. (7) is obeyed (when there are no free surfaces).

We found that the moment equation with $m=0$, Eq. (5), gave a better answer than the higher-m equations, particularly at short wavelengths. This is perhaps due to the presence of the $(DW)^2$ term in the general moment equation. That term is absent only for $m=0$. We know that the slope $(DW)_{\rm class}$ cannot be correct because it is not continuous: $W_{\rm class}$ has a cusp at $y=y^*$, while $W_{\rm exact}$ *and* $(DW)_{\rm exact}$ must be continuous if the density profile $\rho(y)$ is continuous.[7] This explains the discrepancy between the $m=0$ and $m=1$ results which we find at large k because $(DW)_{\rm class}\sim kW_{\rm class}\sim k$ at the peak of the eigenfunction, so that the error in DW becomes more pronounced at larger-k values.

We do *not* use Eq. (7) to evaluate the fastest growth rates: we use it only as a check of consistency. It represents an absolute upper bound and is obtained by optimizing the numerator and denominator of Eq. (5) or Eq. (6) independently. Equation (7) is trivially satisfied, but uninteresting when there is a free surface, $\rho=0$, or when there is a sudden density jump, $D\rho=\infty$, as in the classical case. The point we wish to make is that when $\rho_{\min}>0$ and $D\rho_{\max}<\infty$ then the growth rate, which typically increases as some power of k, eventually has to flatten out and reach an asymptote which satisfies Eq. (7). This was indeed the case for the purely exponential density profile $\rho=\rho_0e^{\beta y}$ which could be solved exactly (see, e.g., Ref. 7), and is also true of the examples treated here whenever there are no free surfaces and no sudden density jumps. Equation (9), on the other hand, is quite restrictive and valid only for $W=W_{\rm class}$. The results presented in this paper satisfy also Eq. (9), because we do use $W_{\rm class}$ in this approximation technique, but the fact that $W_{\rm class}$ is only an approximation and not the exact eigenfunction reveals itself through the m dependence of our results. As stated earlier, growth rates calculated with the exact W do not depend on m.

We tried optimizing simultaneously the numerator and denominator of Eqs. (5) and (6) with respect to W. For $m=0$ we obtain from Eq. (5)

$$\delta\gamma\int W\left[\frac{\rho}{g}+\frac{D\rho}{\gamma^2}\right]dy=\int\delta W\left[\frac{D\rho}{\gamma}-\frac{\gamma\rho}{g}\right]dy\ ,$$

which suggests that $\delta\gamma\sim0$ if $\gamma^2/g=D\rho/\rho$. Strictly speaking, this makes sense only for the purely exponential density profile where $D\rho/\rho=\beta$ is a constant independent of position y. For $m=1$ we obtain from Eq. (6)

$$-\frac{1}{2}\frac{\delta\gamma}{\gamma}\int W\left[D(\rho DW)-k^2\rho W-\frac{gk^2}{\gamma^2}W D\rho\right]dy$$
$$=\int \delta W\left[D(\rho DW)-k^2\rho W+\frac{gk^2}{\gamma^2}W D\rho\right]dy\ ,$$

which was already derived in Ref. 8 (Chap. X, Eq. 94). This equation shows that if W satisfies the original differential equation, Eq. (3), then small variations δW around W do not, to first order in δW, induce a change $\delta\gamma$ in the corresponding γ. As mentioned in Ref. 8, this forms the basis for a variational, albeit numerical, search for γ. We now turn to applications.

III. APPLICATIONS

A. Constant plus exponential density profile

Our first application is the density profile considered in Ref. 6:

$$\rho(y)=\begin{cases}\rho_1+\frac{1}{2}\delta\rho\, e^{\beta y}, & y\le 0\\ \rho_2-\frac{1}{2}\delta\rho\, e^{-\beta y}, & y\ge 0\end{cases} \tag{10}$$

where $\delta\rho=\rho_2-\rho_1$. Unlike the purely exponential density profile, this one cannot be solved analytically. Before using W_{class} to estimate the growth rate, we used our earlier method with $N=52$ to simulate the above density profile and calculate the "exact" eigenfunctions and eigenvalues associated with the largest growth rates. Figure 1 shows these eigenfunctions for $k=4,8,16$. The density profile is also shown in Fig. 1: we have set $\rho_1=1$, $\rho_2=20$, and $\beta=4$.

We see that all the eigenfunctions peak in the $y<0$ region and become more localized as k increases. To obtain a simple analytic expression, however, we shall use W_{class} always peaking at $y=0$, i.e., Eq. (8) with $y^*=0$. For $m=0$ we find

$$\frac{\gamma^2_{[0]}}{g}=\frac{k\beta}{k+\beta}\left[\frac{\rho_2-\rho_1}{\rho_2+\rho_1}\right], \tag{11}$$

which agrees with the expression derived in Ref. 6. Using Eq. (9), we find that the higher moment equations yield

$$\frac{\gamma^2_{[m]}}{g}=\frac{k\beta}{k(m+1)+\beta}\left[\frac{\rho_2-\rho_1}{\rho_2+\rho_1}\right]. \tag{12}$$

While in the limit $k\to 0$, both Eq. (11) and Eq. (12) reduce to the same classical expression in the limit $k\to\infty$:

$$\frac{\gamma^2_{[0]}}{g}\to\beta\left[\frac{\rho_2-\rho_1}{\rho_2+\rho_1}\right], \tag{13}$$

while

$$\frac{\gamma^2_{[m]}}{\gamma^2_{[0]}}\to\frac{1}{m+1}\ . \tag{14}$$

The factor of 2 difference mentioned in our Introduction can be traced to using the moment equation with $m=0$ or $m=1$. The $m=1$ equation can be found in Ref. 8 including surface tension and viscosity.

In Fig. 2 we compare the growth rates $\gamma/\sqrt{g}$ calculated in three different ways: our earlier method with $N=52$, and the present method of using the moment equation with $m=0$ and $m=1$. Clearly, $m=0$ comes closer to the $N=52$ result. The deviation at larger k which persists even for $m=0$ is probably due to the fact that W_{exact} does not peak exactly at $y=0$. However, con-

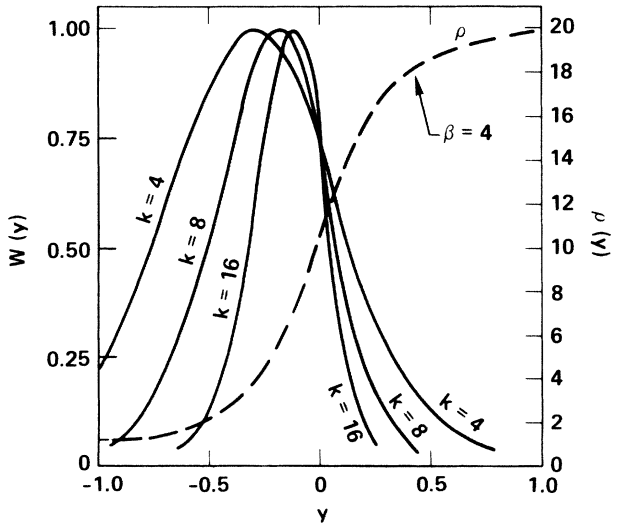

FIG. 1. Constant plus exponential density profile (dashed line) and the eigenfunctions associated with the largest growth rates for $k=4$, 8, and 16, calculated with $N=52$. The scale is set by $\beta=4$.

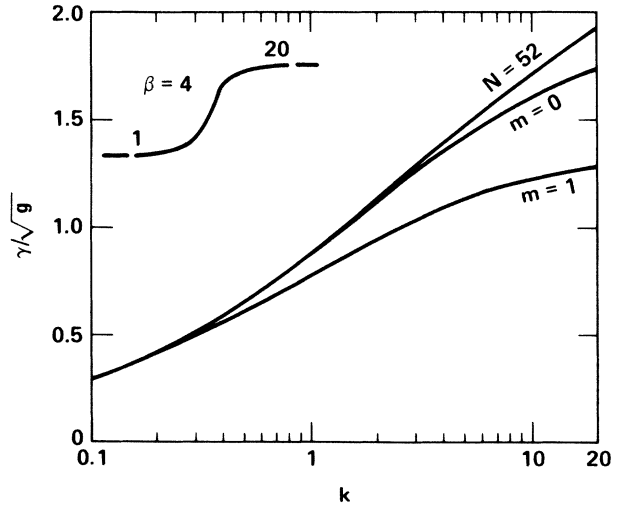

FIG. 2. The growth rate as a function of wave number for the constant plus exponential density profile. The curve labeled $N=52$ is obtained by using 52 fluid layers to represent the density profile (see Fig. 1 for representative eigenfunctions). The curves labeled $m=0$ and $m=1$ are the results of the corresponding moment equations.

sidering the simplicity of Eq. (11), its description of γ over such a fairly wide range of k is quite satisfactory. A similarly good agreement was obtained for the density ratio $\rho_2/\rho_1=2$. As far as we know this is the first time that the accuracy of Eq. (11), first derived in Ref. 6 for this specific density profile, has been checked by a completely different method.

B. Linear density profile

For our next application we chose a linear density profile,

$$\rho(y)=\begin{cases}\rho_1, & y<-d/2\\ (\rho_1+\rho_2)/2+(\rho_2-\rho_1)(y/d), & -d/2\le y\le d/2\\ \rho_2, & y\ge d/2\ .\end{cases} \tag{15}$$

It is worth reporting that our first choice for the eigenfunction was W_{class} peaking at $y=y^*=0$. However, this gave substantially wrong answers (too small growth rates) when the density contrast ρ_2/ρ_1 was large. The choice $y^*=-d/2$ results in the following expression for the growth rate:

$$\frac{\gamma^2_{[0]}}{gk}=\frac{1}{1+2\rho_1 dk(\rho_2-\rho_1)^{-1}(1-e^{-kd})^{-1}}\ , \tag{16}$$

which gave very good agreement with our $N=52$ simulation of a linear density profile with $\rho_1/\rho_2=\frac{1}{20}$. With hindsight the choice $y^*=-d/2$ is clearly preferred since this is the location where $D\rho/\rho$ is maximum. While for long wavelengths this choice does not matter (they all go the classical limit), for shorter wavelengths it is crucial. Indeed, the exact eigenfunctions obtained by our previous $N=52$ method all peak at $y=-d/2$. This is shown in Fig. 3 where we plot the density profile and the eigenfunctions associated with the largest growth rates for $k=4$, 8, and 16. The scale for length is set by $d=1$.

In the limit $d\to 0$ or, alternatively, in the long-wavelength limit, Eq. (16) reduces to the classical result

$$\frac{\gamma^2_{[0]}}{gk}\to\frac{\rho_2-\rho_1}{\rho_2+\rho_1}\quad \text{as } k\to 0\ , \tag{17}$$

while in the short-wavelength limit it reduces to

$$\frac{\gamma^2_{[0]}}{g}\to\frac{\rho_2-\rho_1}{2\rho_1 d}\quad \text{as } k\to\infty\ , \tag{18}$$

which can be seen to coincide with $D\rho/\rho$ at $y=-d/2$. [Note that $D\rho$ is not continuous at $y=-d/2$ and must be obtained by averaging over $D\rho(y=-d/2-\epsilon)=0$ and $D\rho(y=-d/2+\epsilon)=(\rho_2-\rho_1)/d$, hence the factor $\frac{1}{2}$ in Eq. (18).]

Equation (16) was obtained by breaking down the integration region into three parts: $-\infty<y<-d/2$ where $D\rho=0$, $-d/2<y<d/2$ where $D\rho=(\rho_2-\rho_1)/d$, and $d/2<y<\infty$ where $D\rho=0$ again. Equations (16), (17), and (18) are rigorous results, and the factor of $\frac{1}{2}$ in Eq. (18) arises automatically.

It is interesting to point out that if $\rho_1=0$, Eq. (16) reduces to $\gamma^2=gk$. This is, in fact, an exact result valid for all density profiles with a free surface (see Ref. 7). In other words, our choice for W happens to coincide with the exact eigenfunction for that profile if $\rho_1=0$. Consequently this result is independent of m. This would not have been the case if $y^*=0$.

If $\rho_1\neq 0$ then the growth rates depend on m, and we can use Eq. (9) again to relate the higher moments to $m=0$. In Fig. 4 we show the growth rates calculated for $m=0$, $m=1$, and for our $N=52$ simulation of a linear density profile with the ratio $\rho_1/\rho_2=\frac{1}{20}$. The agreement between the $N=52$ method and Eq. (16) is striking.

Such large density contrasts are of interest in ICF targets. For cases where the density contrast is not so large,

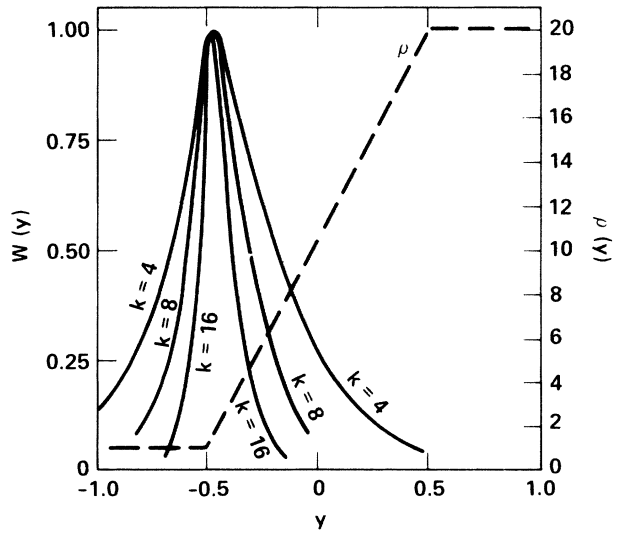

FIG. 3. Same as Fig. 1 for the linear density profile. The scale is set by $d=1$.

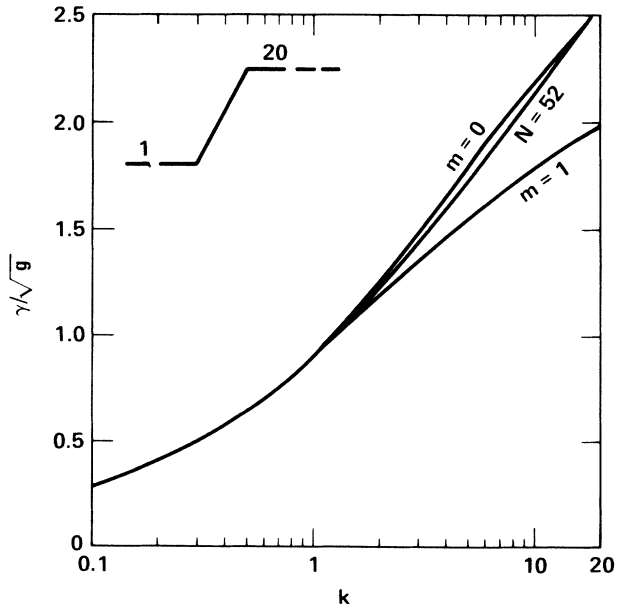

FIG. 4. Same as Fig. 2 for the linear density profile.

i.e., $\rho_1 \sim \rho_2$, Eq. (16) predicts growth rates that are somewhat too small: If $\rho_1 = \frac{1}{2}\rho_2$, then $\gamma_{[0]}$ is about 20% smaller than what the $N=52$ method predicts at short wavelengths, $\lambda \lesssim d/3$. There is no problem at long wavelengths. We found that this discrepancy is due primarily to the *shape* of the eigenfunction rather than the location of its peak: $W_{N=52}$ still peaks close to $y=-d/2$, but is broader than the exponentially decreasing W_{class}.

C. Finite thickness density profile

Our last example illustrates a shell thickness t with density gradient lengths d_1 and d_2 on either side, as shown in Fig. 5. Assuming that $W = W_{\text{class}}$ and that it peaks at the location shown in Fig. 5, we find

$$\frac{\gamma_{[0]}^2}{gk} = \frac{1}{1+2\rho_1 d_1 d_2 k\left[(\rho_2-\rho_1)(1-e^{-kd_1})d_2+(\rho_3-\rho_2)(1-e^{-kd_2})d_1 e^{-k(d_1+t)}\right]^{-1}} . \tag{19}$$

As a check, note that if $\rho_3=\rho_2$ we return to the previous example; similarly if $t=\infty$ or $d_2=\infty$. As in the previous example, setting $\rho_1=0$ gives $\gamma^2=gk$. Since we know that this is an exact result in this case also, we expect and indeed find Eq. (19) to be a good approximation if the density contrast ρ_2/ρ_1 is large.

In the very-long-wavelength limit Eq. (19) reduces to

$$\frac{\gamma_{[0]}^2}{gk} \to \frac{\rho_3-\rho_1}{\rho_3+\rho_1} \quad \text{as } k\to 0 , \tag{20}$$

and in the very-short-wavelength limit

$$\frac{\gamma_{[0]}^2}{g} \to \frac{\rho_2-\rho_1}{2\rho_1 d_1} \quad \text{as } k\to\infty . \tag{21}$$

These results are consistent with the fact that long-wavelength perturbations probe the density profile at larger distances while short-wavelength perturbations, being more localized, see only a limited region of the density profile, hence the similarity of Eqs. (18) and (21).

In Fig. 6 we plot the growth rates γ as functions of k for four different density profiles. These are obtained from our analytic formulas. Profile A is the classical profile. Profile B shows the effects of replacing the sudden density jump of A by a linear density gradient: Profiles A and B overlap at long wavelengths, while at short wavelengths B is considerably more stable than A. Profile C shows the effect of the finite thickness or, alternatively, the presence of a free surface, $\rho=0$, on the other side of a shell. Now, at short wavelengths C and B are identical (the free surface is too far to make any difference), while at longer wavelengths the free surface makes its presence felt by suppressing the growth rate: $\gamma_C < \gamma_B$ for $k \lesssim 1$ (the gradient length $d_1=1$ is used for scale, and we have set $t_1=1$, $d_2=0$). Finally, profile D is the case where both $t=0$ and $d_2=0$, and Fig. 6 shows that while at short wavelengths B, C, and D all have identical growth rates, at longer wavelengths D is even more stable. The reason is that by eliminating t we have brought the stable free surface even closer.

Several special cases can be obtained from Eq. (19). In particular, for $d_1=d_2=0$, it reduces to

$$\lim_{d_2\to 0}\lim_{d_1\to 0}\frac{\gamma_{[0]}^2}{gk} = \frac{1}{1+2\rho_1[\rho_2-\rho_1+(\rho_3-\rho_2)e^{-kt}]^{-1}} . \tag{22}$$

This is, in fact, the case $N=3$: a layer of fluid of density ρ_2 and thickness t between two semi-infinite fluids of densities ρ_1 and ρ_3. An explicit expression for the exact growth rates (there are two) was given in Ref. 7. Equation (22) does not agree with either of them except for trivial cases such as $\rho_1=0$ or $\rho_3=\rho_2$. The reason is two-

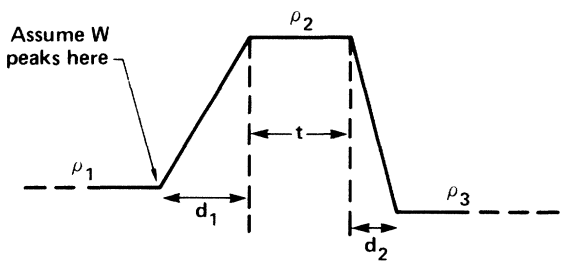

FIG. 5. Finite thickness density profile with linear gradients between three constant densities (see Sec. III C).

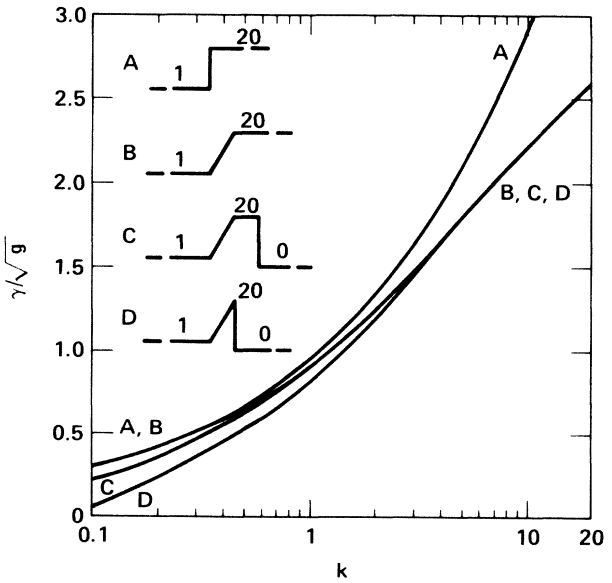

FIG. 6. Growth rates as functions of wave number k for four different density profiles (see text).

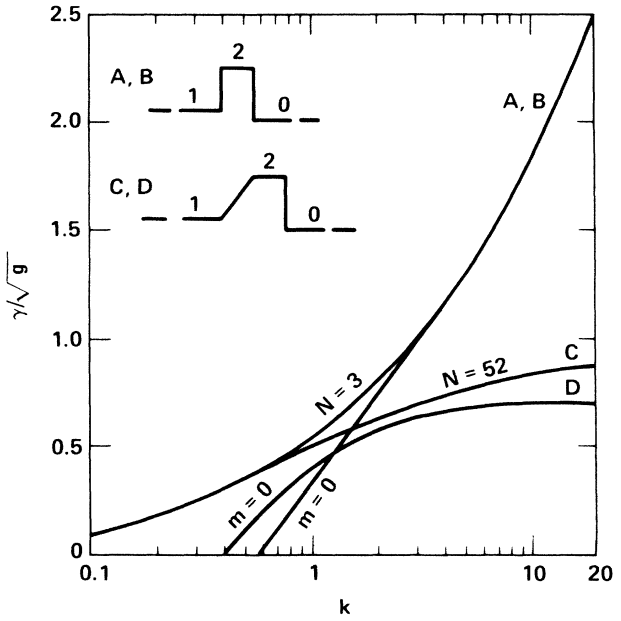

FIG. 7. Growth rates as functions of wave number k for two different density profiles (see text).

fold: (1) In general, the eigenfunctions do not peak at the ρ_1/ρ_2 interface but somewhere between this and the other interface, and (2) the eigenfunctions have both an exponentially decreasing as well as increasing part in the middle layer.

To highlight the difference between our simple analytic formulas and the exact results, we consider the case $\rho_1=\frac{1}{2}\rho_2$ and $\rho_3=0$. Figure 7 shows two density profiles and four growth rates: A and B refer to the same density profile; the curve labeled $N=3$ is the exact result while the curve labeled $m=0$ is based on Eq. (22). The agreement is good at short wavelengths, but bad at long wavelengths. In fact, Eq. (22) becomes negative at $k<0.6$ (the scale is set by $t=1$). While there *is* a stable mode in the exact result given by $\gamma^2=-gk$, there is also a second and dominant mode which never becomes negative.

Curves C and D in Fig. 7 refer to the second density profile where the $\rho=1$ to $\rho=2$ abrupt transition is replaced by a linear density gradient of length $d_1=1$. Curve C is the result of using $N=52$ to simulate this density profile, while curve D is based on Eq. (19) with $\rho_1=1$, $\rho_2=2$, $\rho_3=0$, $d_1=1$, $t_1=1$, and $d_2=0$. There is fair agreement, within 20%, at short wavelengths, while at longer wavelengths $\gamma^2_{[0]}$ again becomes negative, suggesting that the effect of the stable interface between $\rho=2$ and $\rho=0$ is overestimated in these formulas.

We should point out that the small density contrast $\rho_2/\rho_1=2/1$ was chosen in Fig. 7 to highlight where Eq. (19) fails. Indeed, for the larger density contrast used in Fig. 6 we found that Eq. (19) agrees very closely with the $N=52$ results at both long and short wavelengths.

IV. REMARKS AND CONCLUSIONS

We derived simple, explicit analytic formulas for the growth rate of the Rayleigh-Taylor instability in a number of density profiles, and compared the results with our earlier technique. We checked the $N=52$ result by comparing them with $N=27$ and $N=77$.

In all cases we have focused on the *largest* growth rate. There are many growth rates: In the case of finite N, there are $N-1$ growth rates, and in the case of continuous density profiles there are infinitely many growth rates. While all of them are needed to find out how perturbations grow at each interface and feed through from one interface to another,[9] the largest growth rate, which dominates at late times, can be used to assess the impact of a particular density profile and/or compare it with another one.

From the examples considered here it appears that the choice of the classical eigenfunction peaking where $D\rho/\rho$ peaks is a good one, especially when used in the $m=0$ moment equation. One may try other functions or search for the one that maximizes $\gamma_{[1]}$ (this procedure is equivalent to solving the original differential equation—see Ref. 8), but the expressions quickly become too complicated, especially when one tries to take into account the fact that the location of the peak is a function of both density and wavelength, as in Fig. 1.

We end with a brief summary of the present experimental situation: Experiments with lasers[5] show that growth rates are reduced by a factor of about 2 from their classical values. However, one cannot separate the effects of ablation and density gradients. In a more recent classical-type experiment with three fluids, where there is no ablation and the acceleration is provided by rockets, it was found[10] that a middle transitional or antimix layer of density $\rho_2=(\rho_1\rho_3)^{1/2}$ suppresses, to some extent, the mix of the two fluids on each side. The experiments were well into the nonlinear regime and cannot be properly analyzed in terms of a simple linear theory, but they do suggest that density gradients can be a stabilizing factor in Rayleigh-Taylor instabilities.

ACKNOWLEDGMENTS

This work was supported by the U.S. Department of Energy, Contract No. W-7405-ENG-48, and performed under its auspices by the Lawrence Livermore National Laboratory.

[1]Lord Rayleigh, *Scientific Papers* (Dover, New York, 1900), Vol. 2.

[2]G. I. Taylor, Proc. R. Soc. London, Ser. A **201**, 192 (1950).

[3]J. H. Nuckolls, L. Wood, A. Thiessen, and G. Zimmerman, Nature (London) **239**, 139 (1972); S. E. Bodner, Phys. Rev. Lett. **33**, 761 (1974).

[4]R. L. McCrory, L. Montierth, R. L. Morse, and C. P. Verdon, Phys. Rev. Lett. **46**, 336 (1981); M. H. Emery, J. H. Gardner, and J. P. Boris, *ibid.* **48**, 677 (1982); R. G. Evans, A. J. Bennett, and G. J. Pert, *ibid.* **49**, 1639 (1982).

[5]J. D. Kilkenny, J. D. Hares, C. S. Lewis, and P. T. Rumsby, J. Phys. D **13**, L123 (1980); R. R. Whitlock *et al.*, Phys. Rev.

Lett. **52**, 819 (1984); J. Grun *et al.*, *ibid.* **53**, 1352 (1984).

[6]R. Lelevier, G. J. Lasher, and F. Bjorklund, University of California Report No. UCRL-4459, 1955 (unpublished), available from Technical Information Department, Lawrence Livermore National Laboratory, Livermore, California 94550.

[7]K. O. Mikaelian, Phys. Rev. Lett. **48**, 1365 (1982); Phys. Rev. A **26**, 2140 (1982).

[8]S. Chandrasekhar, *Hydrodynamic and Hydromagnetic Stability* (Oxford University Press, London, 1968).

[9]K. O. Mikaelian, Phys. Rev. A **28**, 1637 (1983).

[10]K. D. Burrows, V. S. Smeeton, and D. L. Youngs, United Kingdom Atomic Weapons Research Establishment (AWRE) Report No. O 22/84, 1984 (unpublished).